Performance and reliability testing of an active mooring system for peak load reduction

Journal Title
XX(X):1–11

DOI: 10.1177/ToBeAssigned
www.sagepub.com/

Jamie F Luxmoore[1], Philipp R Thies[1], Simon Grey[2], David Newsam[3] and Lars Johanning[1]

Abstract

Offshore Renewable Energy systems are generally required to operate in exposed offshore locations for long deployment periods at low cost. This requires innovative new mooring systems solutions to go beyond the existing offshore industry designs. A number of novel mooring systems have recently been proposed which de-couple mooring line compliance and minimum breaking load, offering multiple benefits to designers. Demonstrating reliability for such highly novel systems where standards do not yet exist is a common problem both for mooring systems specifically and in offshore renewable applications generally. A performance and reliability test method is proposed here and is applied to a novel mooring system, the Intelligent Active Mooring System (IAMS). IAMS offers line stiffness and damping properties which can be optimised to the prevailing metocean conditions without compromising minimum breaking load, as well as adjustable pre-tension for tidal range compensation or for service access. The paper presents the results of detailed, large-scale physical performance tests that demonstrate load reductions under normal operating and extreme sea state conditions. The rationale and findings for an accelerated reliability test regime that quantifies the ultimate load capacity of the component and gives insight into the governing failure modes are also presented. The presented test approach provides assurance for the overall system integrity.

Keywords

Offshore renewable energy, mooring systems, reliability, performance test, component integrity

Introduction

Developing efficient and reliable mooring systems for floating Offshore Energy Converters (OECs) can be challenging compared to more traditional floating platform mooring system design for a number of reasons. Wave energy OECs need to be sited in areas of high wave energy and will almost always be sited in relatively shallow water (less than $50\,\mathrm{m}$ deep). In these depths the waves will include significant non-linearities and both wave breaking and rogue wave activity may be expected[1]. Additionally, tidal range may be significant relative to water depth and tide-induced currents may be higher than in deeper water locations. Floating tidal current OECs may be in less exposed sites in terms of the wave environment, but the very high tidal current velocities (for example the $2\,\mathrm{MW}$ Scotrenewables tidal turbine has a rated current velocity of $3\,\mathrm{m/s}$) mean that steep and rogue waves are relatively more likely due to wave current interactions. Floating wind energy converters are likely to be sited in deeper water and away from strong currents, but wave energy may be high and the wind induced loads are necessarily high. As all OECs are designed to extract as much energy as possible from the environment and as the top end loads on a mooring system are proportional to the energy extracted[2], the challenge is clear.

The most basic requirement of the mooring system of a floating OEC is to reliably maintain the position of the OEC within certain pre-determined boundaries. A well designed mooring system however can do much more than merely keep the OEC on station. The stiffness of the mooring system can have a very significant effect on the peak and fatigue loading forces on a floating OEC[3–5]. In the case of a floating Wave Energy Converter (WEC), the damping of the mooring

[1]College of Engineering, Mathematics and Physical Sciences, University of Exeter, UK
[2]AWS Ocean Energy Ltd, Inverness, UK
[3]Teqniqa Systems Ltd, London, UK

Corresponding author:
Jamie F. Luxmoore, College of Engineering, Mathematics and Physical Sciences, University of Exeter, Penryn Campus, Penryn, Cornwall, TR10 9EZ, UK
Email: j.f.luxmoore@exeter.ac.uk

system (the energy extracted by the mooring system) can have a direct influence on the energy extraction of the device depending on the design[2;6;7].

The characteristics of a mooring system are determined by the configuration of the mooring lines and the line types employed. Conventional options for line types are chain, wire rope and fibre rope. There are a wide range of mooring line configuration permutations, but they can be catergorised into taut or catenary systems with sub-categories based on the number of lines and the use of floats and weights in the system[8].

The performance requirements for a floating OEC mooring system are to provide high minimum breaking load (MBL), good reliability and adequate position keeping in extreme conditions while still having sufficient compliance to reduce the peak and operating loads on the device[4]. A common solution is to employ fibre ropes, but a small number of alternative designs have been proposed recently which offer significant advantages over fibre ropes, primarily through having a stiffness characteristic which increases with increasing line extension. For example the TfI Mooring Tether[3] has an elastomeric element which gives a soft response in normal operation and a separate stiff compressive element to withstand storm loads. The Seaflex system[9] uses elastomeric elements with a rope as backup in the event of over-elongation. The Exeter Tether[4] is a hollow braided fibre rope with an elastomeric core - the tension load is carried by the rope while the core controls the extension by resisting the reduction in diameter as the rope extends.

This paper describes the reliability and performance testing of a novel mooring system, the Intelligent Active Mooring System (IAMS), which like the above mentioned examples has an axial stiffness that increases with increasing line extension. The unique characteristic of IAMS is that the stiffness can also be varied actively in response to the prevailing metocean conditions. This novel system has multiple potential benefits as outlined in Luxmoore et al.[5], but like any new system needs clear reliability and performance data to justify further development. This paper outlines the performance and reliability test method developed for this novel system, then describes the setup, plans and results of the testing, followed by a discussion and conclusions.

Performance and reliability test method

Cost reductions in marine energy of 50 % to 75 % will be needed in the next 10 years to compete with offshore wind[10]. Improving reliability is one of the key areas that can deliver these cost reductions through increased availability (and hence yield) and reduced operation and maintenance costs[11]. Reliability is often seen as a key risk for the commercial development of OECs, as it directly impacts investment decisions. Considerable investment is necessary to build the required prototypes and fund the development programmes to improve the reliability and hence reduce the risks. The investment hurdle can be partially overcome by improving component reliability as lower investment is required for individual component development and reliable components have the potential to be used across multiple OEC designs.

Reliability is “the ability of an item to perform a required function, under given environmental and operational conditions and for a stated period of time” according to ISO8402[12]. The reliability testing method suggested here is based on a Physics of Failure based approach, combining understanding of the likely failure mechanisms with knowledge of the component loading[11]. With novel components where there is little or no data available from similar systems it is necessary to understand the physical principles of operation in order to derive the likely failure mechanisms. Testing should then explore the failure mechanisms under the expected environmental and operating conditions. The aims of the performance and reliability testing are therefore to characterise the performance of IAMS as well as to identify and to study the main failure mechanisms.

Failure modes identification for IAMS

The performance and reliability test method described is applied here to the Intelligent Active Mooring System (IAMS). The IAMS design is based around a hollow braided rope made of Vectran (a high performance multi-filament yarn spun from liquid crystal polymer) which supports all the lengthwise loads. A stainless steel clamping mechanism with integrated internal hydraulic pipe is attached to the braid at each end. The clamp holds both the braid and an internal bladder in place with separate clamping mechanisms for each and also provides a mounting point for shackles to the rest of the mooring system. The flexible water filled bladder inside the hollow braid resists reductions in the braid diameter through hydraulic pressure. As the rope extends, the diameter of the hollow braid decreases until the rope strands finally lock together at around 17° braid angle; any further extension beyond this point is due to the extension of the rope strands. Braid angle α is defined as half the included angle between two crossing strands. A detailed view of the braid fibres is shown in figure 1. A hydraulic accumulator is attached by hydraulic pipes to the bladder outlet so that the

load-extension properties of the whole system can be varied by changing the accumulator air volume and pressure.

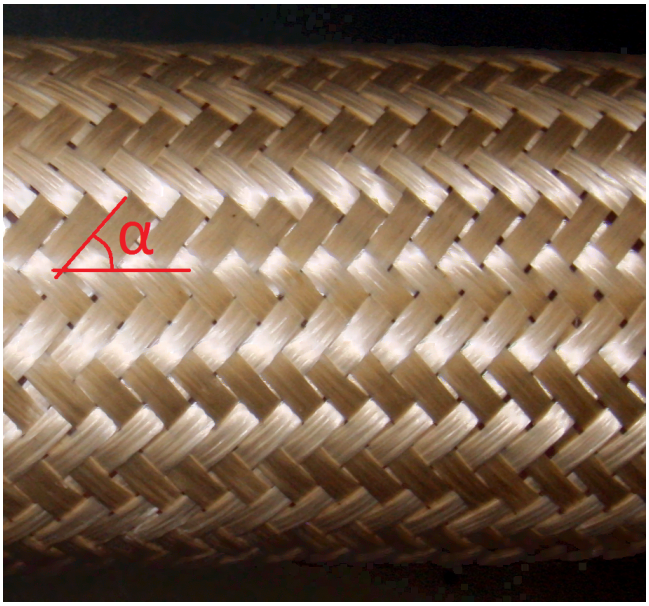

Figure 1. Detailed view of the 32 strand hollow braided Vectran rope, nominal diameter $120\,\mathrm{mm}$. Braid angle α is shown for reference.

The principle failure mechanisms expected are as follows:

1. Burst failure of the bladder due to overpressure or puncturing - the bladder is supported by the braid fibres, but if the pressure increases sufficiently to force the braid fibres apart then a bubble of the bladder material may push through the braid strands causing rupture failure. A simple puncture by a sharp object would have a similar effect.
2. Failure of the end clamping arrangement due to excessive tension - the braid may pull out of the end clamp or may fail at the end clamp due to increased local loading due to the small radius edges.
3. Failure of the braid due to friction induced wear of the braid fibres on themselves or on the end clamp.
4. Failure of the bladder due to friction induced wear on the bladder by the braid fibres or the end clamp.

The predicted failure mechanisms were tested by applying modelled field load profiles to give an improved understanding of the reliability of the prototype design under simulated environmental and operational conditions.

Loading from slack can be a significant problem for certain types of mooring line as it can lead to high snatch loads, stressing both the mooring line and the floating device[3]. The tests used in the reliability assessment therefore cover repeated peak loading (representing extreme wave groups), loading from slack and simulation of extreme sea states; as well as the typical sea simulation tests aimed to assess the performance reliability under normal operating conditions.

Test setup and instrumentation

A prototype of IAMS was constructed by Teqniqa Systems Ltd. The prototype is a nominal $120\,\mathrm{mm}$ in diameter and $2.35\,\mathrm{m}$ long at $45°$ braid angle. It was tested by the University of Exeter at the Dynamic Marine Component (DMaC) test facility, which is a purpose built test rig that aims to replicate the forces and motions that components are subjected to in offshore applications. Tension and position are recorded through the DMaC control system (NI Compact RIO) at $250\,\mathrm{kHz}$ and $120\,\mathrm{kHz}$ respectively (for full details of DMaC capabilities see Johanning et al.[13]). Figure 2 shows the IAMS physical model installed in DMaC.

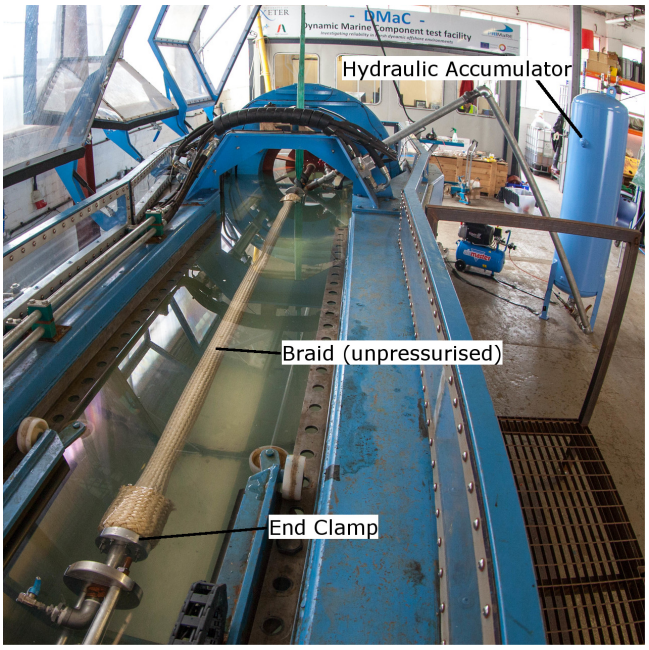

Figure 2. IAMS installed in DMaC

The pressure supply system used in the physical model tests is not representative of the proposed final design, rather it was a bespoke design for this test programme. A schematic of the pressure supply system is shown in figure 3. The braid outlet digital pressure transducer records at $10\,\mathrm{Hz}$, while the digital pressure and temperature transducers on the accumulator record at $2.5\,\mathrm{Hz}$. Emergency pressure relief valves were also fitted. The main constriction in the pipework was a globe valve which caused significant pressure drop. The effects of the pressure drops in the pipework are discussed in some detail below as they impact on the applicability of the results.

The tests run in the DMaC rig were all displacement driven, which is straightforward for the sinusoidal range of

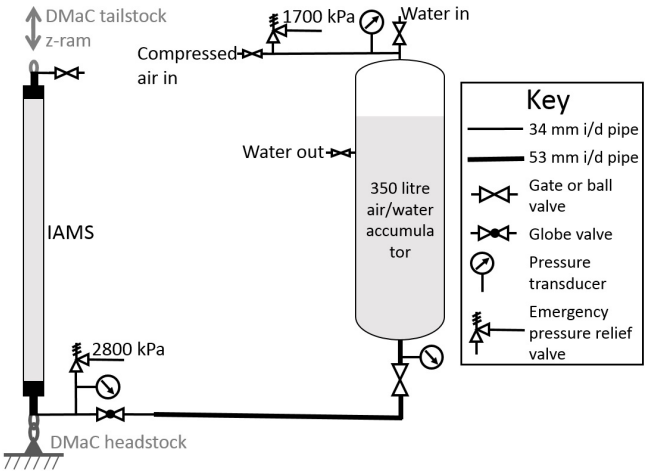

Figure 3. Pressure supply system for physical model test at DMaC

motion studies, but in order to simulate realistic wave driven extensions a model is required. A detailed description of the models and validation results used to generate the wave inputs can be found in Luxmoore et al.[5], a brief summary of the process used to generate the modelled displacement time history is given here.

An analytical model describing the theoretical performance of the IAMS braid and bladder combination was used to simulate the stiffness of IAMS. This was then validated against the physical scale model installed in DMaC by running very long period extension tests to give a baseline, effectively static, performance characteristic. This was used to tune the analytical model to give a validated static load extension relationship. The resulting load extension curve was used to represent IAMS in a hydrodynamic system model. The hydrodynamic model was run using Orcaflex[14] version 9.8a with a model of the South West Moorings Test Facility (SWMTF) buoy and mooring system[15]. The SWMTF buoy is an instrumented ocean buoy designed to provide data to reduce the uncertainties in reliability and cost estimates for moored OECs. The dynamic model of SWMTF without IAMS was first validated against data recorded on SWMTF and then IAMS was substituted in in place of a section of braided nylon mooring line. The model was run for a typical sea state and for an extreme sea state. The extension of 2 m of the modelled section of IAMS was extracted and used to create a displacement time history to drive DMaC.

A comprehensive test schedule was developed to investigate the dynamic performance as well as the reliability and durability of IAMS in a range of simulated predicted operating conditions. The tests were all run at DMaC with the exception of the long duration durability testing, which was completed by Teqniqa Sytsems Ltd on a purpose built test rig. An overview of the tests run at DMaC is shown in table 1. All the tests were repeated for all four combinations of accumulator pressure (directly related to the pre-load at $\alpha = 45°$) and air volume. The pressure / air volume combinations (termed 'configurations') were used in the tests to provide a range of load extension curves to demonstrate part of the performance envelope. The configurations used in the performance assessment are shown in table 2 and the associated validated load-extension curves are shown in figure 4.

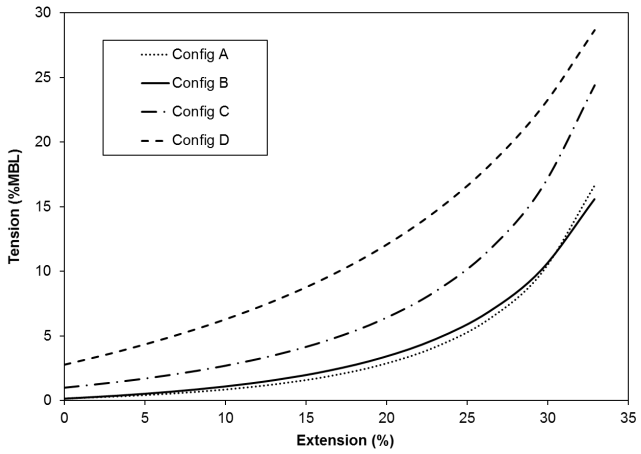

Figure 4. Predicted tension-extension curves for the four configurations used in the performance assessment

In the event of a bladder burst in service, IAMS would continue to act as a rope, with the intention that the device would not break free of its moorings, although the shock loads would be significantly increased as IAMS is much stiffer in un-pressurised form. Under this scenario, the IAMS device becomes effectively a Vectran rope. The braid was therefore tested based on a standard rope test proceedure ISO 18692[16]. The tests could not be fully compliant with the ISO standard, as firstly the ISO standard calls for three identical new specimens and secondly it requires a previously established minimum breaking load (MBL) which was not available at the time. In the absence of an MBL the proof test strength was used. An outline of the test derived from the ISO standard is shown here.

1. Pull to 50 % MBL at 10 % MBL per minute and hold for 30 min
2. 100 cycles at 10 to 30 % MBL at 30 s period.
3. 100 cycles at 20 to 30 % MBL at 10 s period.
4. 100 cycles at 30 to 40 % MBL at 10 s period.
5. 100 cycles at 40 to 50 % MBL at 10 s period.
6. Pull to failure or twice MBL at 20 % MBL per minute

Test	Test aim	Period (s)	Cycles	Extension	Tests per config.
Baseline	Bedding in, static performance	60	1	0-30%	6
Performance	Define load extension curve for model validation	10	5	0-33%	5
Hysteresis	Assess time dependant behaviour	10, 6, 4	20	0-30%	9
Typical sea state	Assess performance and fatigue in realistic ocean conditions	$T_p = 6.71$	35 mins	Irregular	1
Snatch tests	Test response to slack mooring line	8, 6, 5, 4	5	-9-5%	4
Extreme sea state	Assess performance in realistic ocean conditions	$T_p = 8.17$	2 mins	Irregular	3
Semi-static	Assess performance in semi-static conditions	30-300	1 - 3	0-30%	4
Failure state	Single system failure tests - bladder burst	Based on ISO 18692 as detailed below			

Table 1. Overview of tests run at DMaC facility

Configuration	Accumulator air volume (litres)	Pre-load (kN)
A	28.6	0.16
B	33.6	0.16
C	33.6	1.00
D	50.4	2.8

Table 2. Accumulator air volume and pre-load combinations used in the performance assessment.

Results

This section describes the results of the performance and reliability testing; first the necessary correction due to the pressure loss is described, followed by the results of the dynamic performance testing and finally the reliability and durability testing. The critical measures of the dynamic performance of IAMS are the stiffness and the energy dissipated. In this paper the stiffness is presented as the axial rigidity EA (where E is the Young's modulus and A is the cross-sectional area), which is the slope of the tension-strain curve, or the force required to double the length of the sample. The shape of the stiffness curve is also of interest. The energy dissipated by the device gives a measure of the damping provided by the device to the mooring system[2], but does not include damping from other sources in the mooring system such as hydrodynamic damping in a catenary mooring system. The results cover the performance under predicted operating conditions and both single system failure mode operation and fatigue testing.

Correction due to pressure loss

The pressure drop due to the pressure supply system in the test rig had a significant influence on the results which is unrepresentative of the planned final design. The final design will have a much shorter pressure supply system with very little pressure drop at all predicted. As the pressure was recorded at each end of the pressure supply system (albeit at low frequency) it is possible to correct the results to remove the effects of the pressure supply system. The braid angle α can be calculated as:

$$\alpha = \arccos\left(\frac{L_0 + z}{L_F}\right) \tag{1}$$

where z is the elongation of IAMS, L_0 is the hollow braid length at 0% extension and L_F is the helical length of the braid fibres (equal to the theoretical braid length at $\alpha = 0$). Using the recorded pressure p, the tension due to the pressure T_p at one end of the pressure system is:

$$T_p = pA(2/(\tan\alpha)^2 - 1) \tag{2}$$

where $A = A_0(\sin\alpha/\sin\alpha_0)$, A_0 is the cross-sectional area at $0\,\%$ extension and α_0 is the braid angle at $0\,\%$ extension. The corrected tension is then the recorded tension minus the difference between T_p at the braid outlet and the accumulator inlet, assuming zero loss in the pipework system. This correction will not be perfect at high frequency as the pressure gauges recorded at $2.5\,\mathrm{Hz}$ minimum, but for metrics over a full extension - contraction cycle such as the stiffness, the accuracy of the correction will be good; these metrics have therefore been used where possible.

The energy dissipated by the whole system E_{d_0} (which is the same as the damping of the whole system) can be calculated from the area under the load-extension curve (estimated by trapezoidal integration) on the extension-stroke E_{load} minus the area under the load extension curve

on the contraction-stroke E_{unload}[17]:

$$E_{d_0} = E_{load} - E_{unload} \tag{3}$$

in other words the area contained within the hysteresis loop.

An equivalent 'pressure load' at each end of the pipework can be calculated by multiplying the pressure p at each end of the pipework by the instantaneous cross-sectional area A of IAMS. Integrating for the area under the 'pressure load'-extension curve at each end of the pipework and subtracting the two values gives the difference in energy at each end of the pipework in the load $E_{p_{load}}$ and unload $E_{p_{unload}}$ part of the cycle. The energy dissipation due to pressure loss in the pipework E_{d_p} is:

$$E_{d_p} = E_{p_{load}} - E_{p_{unload}} \tag{4}$$

The corrected energy dissipation E_d is then

$$E_d = E_{d_0} - E_{d_p} \tag{5}$$

The results presented below have all been corrected according to the method described above.

Dynamic performance

The results shown here give an overview of the dynamic performance of IAMS.

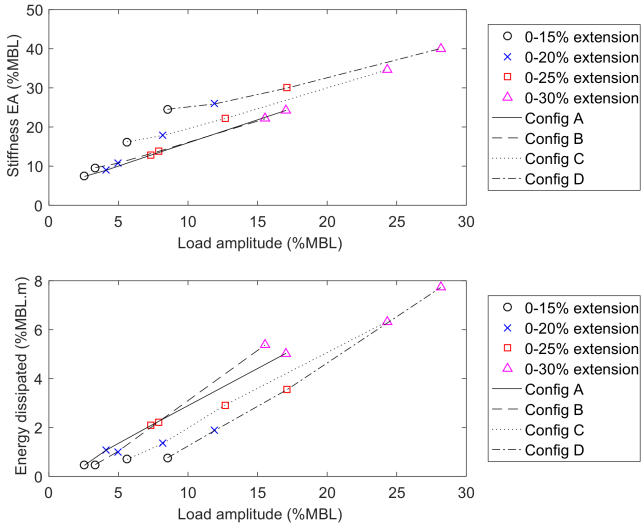

Figure 5. Mean load amplitude plotted against mean stiffness and mean energy dissipated at 10 s period for all 4 configurations.

Figure 5 shows the effect of load amplitude on stiffness and energy dissipated at a fixed frequency of 0.1 Hz for different extension ranges. Stiffness increases with increasing load amplitude for all ranges of extension, but the rate of increase (the steepness of the trend) decreases with increasing range of movement. The energy dissipated increases slightly with increasing load amplitude and more strongly with increasing range of motion.

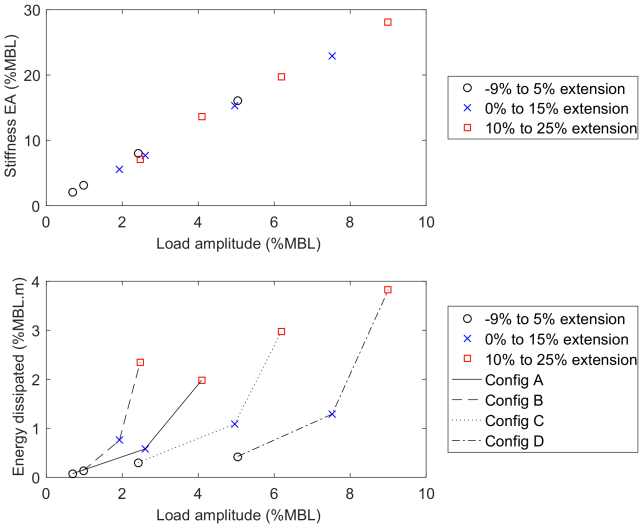

Figure 6. Mean load amplitude plotted against mean stiffness and mean energy dissipated at 10 s period for all 4 configurations.

Figure 6 shows the effect of load amplitude on stiffness and energy dissipated for tests with partial extension. All tests are for 15 % extension, but the starting position is different – the red squares are for tests starting partially extended at 10 % extension while the black circles are for snatch tests starting at slack, i.e. −9 % extension. A smooth transition from slack to under tension was observed in all the tests. The stiffness increases linearly with increasing load amplitude and shows a general increase with increasing pre-load. The energy dissipated increases with increasing starting extension and with increasing accumulator air volume.

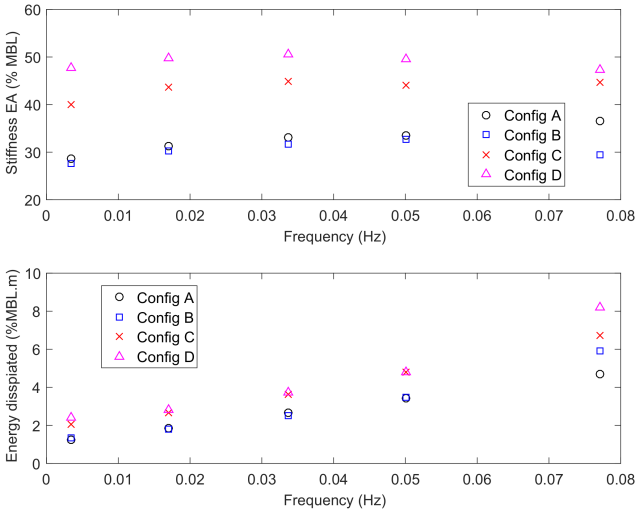

Figure 7. Effect of load application rate on stiffness and energy dissipation. Data is for all 4 configurations over the full range of extension (0 % to 33 %).

Figure 7 shows the effects of the rate of load application on the stiffness and energy dissipation. This figure describes the tests where the full range of normal operation was used, so from 0 % to 33 % extension. The stiffness is largely constant with frequency for each of the configurations. The pre-load has a strong influence on the stiffness, noting that the pre-load is directly related to the starting pressure. The energy dissipation increases with increasing frequency, although note that these tests are all at relatively low frequency (period range is 5 min to 14 s). Higher frequency tests were not possible at the full extension range as the tension went considerably above the planned limit of 40 %MBL at 10 s period. The nominal load limit was chosen to provide a factor of 2.5 safety margin in the pressurised tests based on the static proof test load. There is a small increase in energy dissipated due to increasing pre-load.

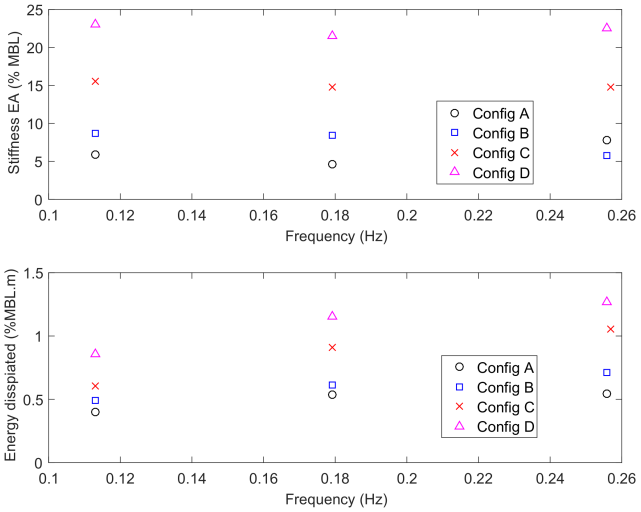

Figure 8. Effect of load application rate on stiffness and energy dissipation. Data is for all 4 configurations over reduced range of extension (0 % to 15 %).

Figure 8 shows the effects of the rate of load application on the stiffness and energy dissipation for a reduced range of motion, but at higher frequency than figure 7. The same trends noted above continue at the higher frequencies (equivalent to roughly 4 s to 10 s period).

Reliability and durability

The reliability test approach has been described above and the main results are presented here.

Figure 9 shows the results of the typical sea state tests. The performance of IAMS follows the predicted performance curve closely throughout each of the 35 min trials for all four configurations. The deviations from the predicted curve visible at the largest extensions are due to the pressure loss correction method, which as stated above is reliant on pressure gauge measurements at 2.5 Hz. This

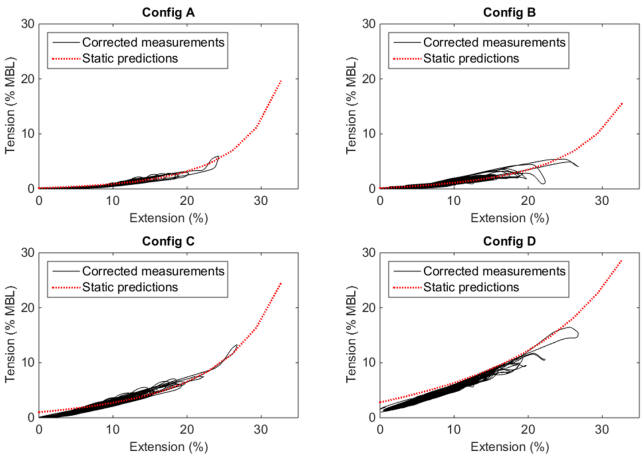

Figure 9. Tension - extension curves in a typical sea state compared to analytical model predictions for configurations a to d

means that where the pressure is changing most rapidly (at the peak extension) the correction method is least reliable. Nonetheless, the data below the extreme follows the predicted curve very closely.

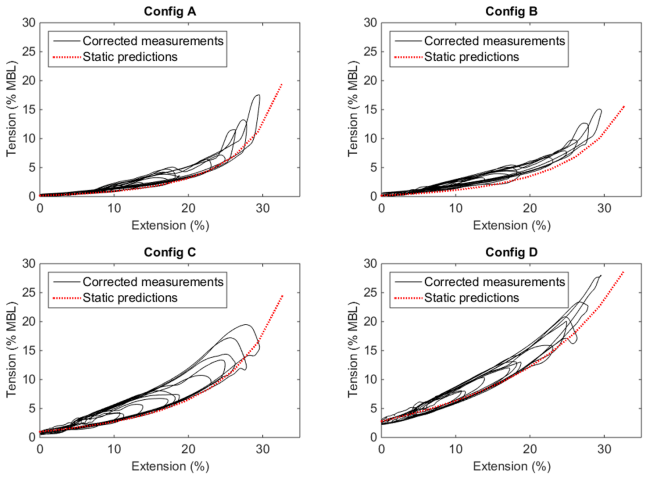

Figure 10. Tension - extension curves in an extreme sea state compared to analytical model predictions for configurations a to d

For the extreme sea state tests a storm condition has been chosen to represent a 1 in 100 year event at the SWMTF buoy site with a 10 m section of IAMS in place on each of the three mooring lines. Figure 10 shows that in all cases the load-extension curve of IAMS compares well to the analytical model predictions. The force is elevated slightly above the analytical prediction as the analytical model does not take braid on braid friction of the outer rope into account, nor does the pressure correction remove all of the pipework effects as there is still a small section of pipework between the braid and the braid end pressure gauge. Given these considerations, the response is very similar to the analytical model prediction and gives confidence that IAMS will perform as expected in extreme storm conditions.

Four principle failure mechanisms have been identified in the failure modes analysis; i) burst failure of the bladder due to overpressure or puncturing, ii) failure of the end clamping arrangement due to excessive tension, iii) failure of the braid due to friction induced wear on the braid fibres and iv) failure of the bladder due to friction induced wear on the bladder by the braid fibres or the end clamp.

Bladder failure due to overpressure (failure mechanism i)) occurred early in the testing programme at $640\,\mathrm{kPa}$. This test was conducted with very low tension on the braid, which allowed a bubble of the bladder material to push through the braid. Static pressure was subsequently limited to $300\,\mathrm{kPa}$, although the internal pressure under dynamic loading (caused by applying tension to the braid rather than increasing the static pressure) frequently exceeded $700\,\mathrm{kPa}$ during the testing without further failure. Bladder failure due to puncture was not assessed during the testing. Failure mechanism ii), the end clamping arrangement was tested by static pull prior to the main test phase to set the initial proof load, which was then adopted as the Minimum Braking Load (MBL) for all subsequent tests.

Failure mechanisms iii) and iv) were both assessed by endurance testing. Two braid samples were cycled between $22°$ and $46°$ braid angle at a tensile load of $5.25\,\mathrm{t}$ and a static pressure of $200\,\mathrm{kPa}$ for $500\,000$ cycles. The samples were microscopically examined before and after the testing. No significant signs of abrasion were detected. A sample of the braid fibres after the endurance testing is shown in figure 11.

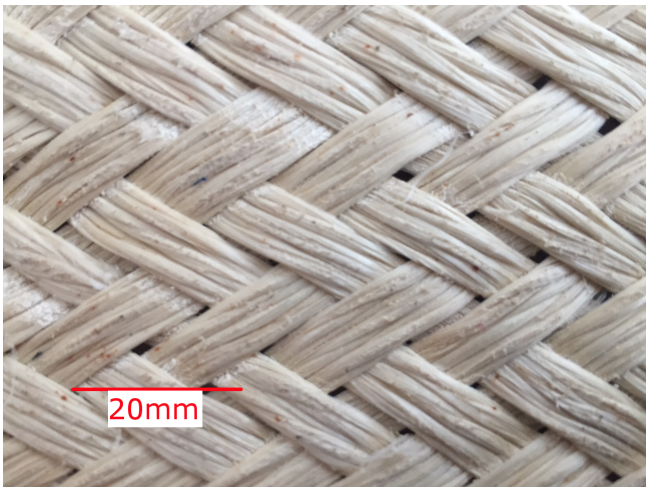

Figure 11. Detail of braid fibres after $500\,000$ cycles

A fourth failure mechanism was identified during the testing which ultimately resulted in bladder failure, but was caused by a local change in the braid angle causing a constriction in the braid at a choke point and associated expansion of the braid to either side (shown in figure 12). This mechanism is described as ‘waisting and bellying’ was the most significant failure mechanism and resulted in the failure of the second prototype. The mechanism results in a bubble or blister of the bladder material showing through the braid at the expansion point. The normal working of the braid fibres then causes a scissoring motion which cuts the bubble open.

Figure 12. Waisting and bellying of the braid fibre with original 32 strand braid observed at $300\,\mathrm{kPa}$ during testing

The waisting and bellying effect became visible after a few hundred cycles for all variants of end clamp design and bladder material tested with the 32 strand $120\,\mathrm{mm}$ braid. A finer weave of the braid material (a braid containing the same weight of material and equivalent tensile performance but more strands) was found to eliminate the problem achieving over $10\,000$ cycles in the endurance testing with no effect apparent (see figure 13).

Figure 13. Fine weave braid after endurance testing

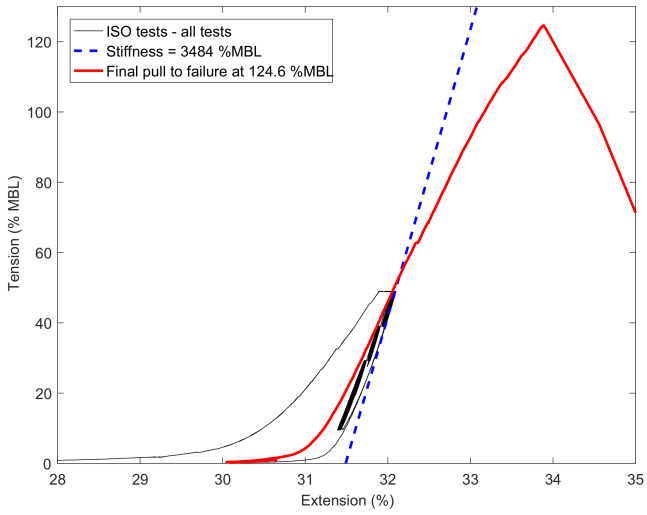

Figure 14. Unpressurised test to failure - performance as a rope

Figure 14 shows the results of a failure mode test simulating performance post bladder burst. Static creep at 50 %MBL was 0.2 % of the static length in 30 min. The stiffness was 3485 kN, based on the mean of the final three 40 % to 50 % extension tests at 10 s period. Final failure occurred at 124.6 %MBL. This is the second of two tests, the results of the first test were similar, giving a stiffness of 3570 kN and final failure at 112 %MBL. In both cases the final failure was due to the braid strands pulling out of the end clamping arrangement.

Discussion

This section discusses the method and results of the performance and reliability testing carried on IAMS. Testing component performance and reliability can help to de-risk OEC development projects, easing investment decisions and hence helping to push the industry forward. The reliability test method used combines the understanding of both the expected component loading environment and the physics of the component failure mechanisms. This method has been applied to design a test programme aimed at characterising the failure mechanisms and performance envelope. The component under test is the Intelligent Active Mooring System (IAMS), a proposed mooring line component that can reduce the loads on floating OECs[5] by means of a non-linear axial stiffness that can be varied in response to the prevailing metocean conditions.

The semi-static (very low frequency) performance of IAMS is similar to that predicted by the analytical model as reported in Luxmoore et al.[5]. The performance under dynamic conditions is slightly more complex as there are several factors that influence the behaviour and the additional hysteresis caused by the test setup (the pressure supply system) has to be accounted for to ensure representative results. A correction based on the analytical model and using the measured pressure at each end of the pipework has been applied to all the results presented above.

The critical measures of the dynamic performance of IAMS are the stiffness and the energy dissipated. Stiffness increases with increasing load amplitude, while the energy dissipated increases more strongly with increasing range of motion. The stiffness shows a general increase with increasing pre-load. The energy dissipated increases with increasing starting extension and with increasing accumulator air volume. The load application frequency also has an effect on the performance. The stiffness is largely constant with frequency for each of the configurations, but the energy dissipation increases with increasing frequency.

The starting extension has a strong influence on the performance. IAMS shows a very smooth transition from slack to under tension, which will help considerably to reduce the shock loads on a mooring system. The stiffness at a fixed range of motion increases with increasing starting tension, once the slack has been taken out of the system. Likewise the energy dissipated also increases as the starting tension increases beyond the slack condition for a fixed range of motion.

The reliability tests were designed to represent realistically scaled extreme and normal operating conditions. The response of IAMS throughout the reliability testing showed that the response is similar to the analytical model predictions throughout the performance envelope. This gives confidence that IAMS units can be designed to operate reliably in the conditions likely to be encountered by floating Offshore Energy Converters in a range of installation locations provided that the local conditions are well understood. These results do not show how IAMS will scale as all the tests were performed with a 2 m long 120 mm diameter prototype, but they do show that the analytical prediction model is reliable at this scale and give confidence in the analytical model at different scales.

The tendency for the braid fibres to bunch together during working forming a marked narrow section significantly impacted the durability of the design. This waist is accompanied by a clear belly, a wider section before the braid returns to a more consistent diameter. The strands at the belly are inevitably further apart than they are over the rest of the length. This forms small diamond shaped gaps in the braid covering of the bladder (see figure 12). As the bladder is made of a stretchable material, small blisters of the bladder material push through the diamond shaped gaps. As the braid

angle changes the edges of the diamond shaped gaps in the braid fibres scissor together resulting in a burst failure of the bladder. This phenomenon of local braid distribution change is not reported elsewhere with similar structures to the authors' knowledge, and may be unique to this particular architecture and usage pattern. In an effort to understand this wasting and bellying phenomenon better, the braid geometry was studied in more detail. Reducing the strand or bundle mass, effectively a finer weave with the same overall braid diameter, was found to be an effective solution. This modified braid geometry was introduced into the endurance cycling braid test and has been shown to eliminate the bellying phenomenon up to 10 000 cycles. Investigation into the potential use of Finite Element Analysis to define and accurately characterise the mechanical behaviour of the braid interaction has been proposed, and will take place as part of future enhancements.

Reliability of the braid itself is likely to be high as almost no braid fibre wear could be detected after 500 000 cycles. The single system failure state analysis with a burst bladder showed that the mechanical parts of IAMS performed as expected. The braid exhibits very low creep and a very stiff response of around 3500 kN. The breaking loads of the two specimens tested both give a safety factor for the end clamping arrangement of over 4 compared to the predicted peak loads at prototype scale.

Conclusions

The paper has described and demonstrated a performance and reliability test approach that is suitable to ensure component compliance and integrity at early design stages. This methodology of combining available and/or modelled field load profiles to physically replicate and emulate operational and extreme load conditions will not only prove useful for mooring system developments, but could assist in technology development for OECs in general. Technology innovations have to satisfy the justified investor and end-user scrutiny. A collaborative effort to facilitate component and system assurance tests may assist in this.

Applying the approach to IAMS has shown that the governing failure modes for IAMS could be confirmed, assessed and largely mitigated through refined technical design and manufacturing specifications.

The confirmed physical performance and adjustable non-linear stiffness (the load extension behaviour) is a promising result for this novel mooring component. The mitigation of peak loads is physically achievable at scale. The load absorbing capacity has also demonstrated that the component is capable of reducing snatch loads and acting efficiently as a 'shock absorber' in the mooring system. This holds promise to improve the efficiency of mooring system design, as the reduction of peak and snatch loads will allow the design of systems with relatively lower MBL, and thus lower cost, whilst maintaining overall mooring system integrity levels.

Further work

The fine stranded braid alleviated the waisting and bellying problem to at least 10 000 cycles, but further study is required to define the specific braid architecture to maintain an even braid distribution for long term use.

Acknowledgements

The work reported here is part of a joint project between AWS Ocean Ltd., Teqniqa Systems Ltd. and the University of Exeter. The project was funded in part by the Technology Strategy Board (now Innovate UK) grant number 101970.

References

1. Dysthe K, Krogstad HE and Müller P. Oceanic Rogue Waves. *Annu Rev Fluid Mech* 2008; 40(1): 287–310. DOI:10.1146/annurev.fluid.40.111406.102203.
2. Johanning L, Smith GH and Wolfram J. Measurements of static and dynamic mooring line damping and their importance for floating WEC devices. *Ocean Eng* 2007; 34(14-15): 1918–1934. DOI:10.1016/j.oceaneng.2007.04.002.
3. Thies PR, Johanning L and McEvoy P. A novel mooring tether for peak load mitigation: Initial performance and service simulation testing. *Int J Mar Energy* 2014; 7: 43–56. DOI:10.1016/j.ijome.2014.06.001.
4. Gordelier T, Parish D, Johanning L et al. A novel mooring tether for highly dynamic offshore applications; mitigating peak and fatigue loads via selectable axial stiffness. In *Proc. 4th Int. Conf. Ocean Energy*. Glasgow, p. 10.
5. Luxmoore JF, Grey S, Newsam D et al. Analytical Performance Assessment of a Novel Active Mooring System for Load Reduction in Marine Energy Converters. *Ocean Eng* 2016; 124: 215–225. URL http://www.sciencedirect.com/science/article/pii/S0029801816302955.
6. Vicente PC, De AA, Gato LMC et al. Dynamics of arrays of floating point-absorber wave energy converters with inter-body and bottom slack-mooring connections. *Appl Ocean Res* 2009; 31(4): 267–281. DOI:10.1016/j.apor.2009.09.002. URL http://dx.doi.org/10.1016/j.apor.2009.09.002.
7. Zanuttigh B, Angelelli E and Kofoed JP. Effects of mooring systems on the performance of a wave activated body energy

converter. *Renew Energy* 2013; 57: 422–431. DOI:10.1016/j.renene.2013.02.006.

8. Weller S, Johanning L and Davies P. Best practice report - mooring of floating marine renewable energy devices. Technical report, MERiFIC Deliverable report 3.5.3, 2013.
9. Bengtsson N and Ekström V. Increase life cycle and decrease cost for navigation buoys. Technical report, Seaflex Buoy mooring system, 2010.
10. Low Carbon Innovation Coordination Group. Carbon Innovation Coordination Group Technology Innovation Needs Assessment (TINA) Marine Energy Summary Report. Technical Report August 2012, Low Carbon Innovation Coordination Group, 2012. URL www.lowcarboninnovation.co.uk/document.php?o=7.
11. Thies P, Johanning L, Karikari-Boateng K et al. Component reliability test approaches for marine renewable energy. *Proc Inst Mech Eng Part O J Risk Reliab* 2015; 229(5): 403–416. DOI:10.1177/1748006X15580837. URL http://pio.sagepub.com/lookup/doi/10.1177/1748006X15580837.
12. International Standards Organisation. Quality management and quality assurance – Vocabulary. Technical report, ISO 8402:1986. WITHDRAWN, 1986.
13. Johanning L, Thies PR, Parish D et al. Offshore reliability approach for floating renewable energy devices. In *ASME 2011 30th Int. Conf. Ocean. offshore Arct. Eng.* American Society of Mechanical Engineers, pp. 579–588.
14. Orcina Ltd. Oracflex Version 9.8a Help Documentation, 2015. URL http://www.orcina.com/SoftwareProducts/OrcaFlex/Documentation/Help/.
15. Johanning L, Spargo A and Parish D. Large scale mooring test facility - A technical note. In *Proc. 2nd Int. Conf. Ocean Energy*. Brest, France, p. 10 pp.
16. International Standards Organisation. Fibre ropes for offshore station keeping - polyester. Technical report, ISO 18962:2007(E), 2007.
17. Weller SD, Davies P, Vickers AW et al. Synthetic rope responses in the context of load history: Operational performance. *Ocean Eng* 2014; 83: 111–124. DOI:10.1016/j.oceaneng.2014.03.010.